Disruption Mitigation Using High-Pressure Noble Gas Injection on DIII–D

D.G. Whyte,[1*] T.C. Jernigan,[2] D.A. Humphreys,[3] A.W. Hyatt,[3] C.J. Lasnier,[4] P.B. Parks,[3] T.E. Evans,[3] P.L. Taylor,[3] A.G. Kellman,[3] D.S. Gray,[1] E.M. Hollmann[1]

[1]University of California, San Diego, 9500 Gilman Drive, La Jolla, California 92093
[*]Current address: University of Wisconsin-Madison, Madison WI USA 53706
[2]Oak Ridge National Laboratory, P.O. Box 2008, Oak Ridge, Tennessee 37831
[3]General Atomics, P.O. Box 85608, San Diego, California 92186-5608
[4]Lawerence Livermore National Laboratory, P.O. Box 451, Livermore, California 94551

Abstract. High-pressure gas jet injection of neon and argon is used to mitigate the deleterious effects from tokamak disruptions. Thermal loading of the divertor surfaces, vessel stress from poloidal halo currents and the buildup and loss of relativistic electrons to the wall are all greatly reduced or eliminated. The gas jet penetrates through to the central plasma as a neutral species at its sonic velocity ~ 300–500 m/s. The injected impurity species radiate >95% of the plasma stored energy, accompanied by a 500-fold increase the total electron inventory in the plasma volume, thus decreasing localized heating at the divertor targets. The poloidal halo currents at the wall are reduced because of the rapid cooling and the slow movement of the plasma toward the wall during the current quench. When a sufficient quantity of gas is injected, the extremely large total (free + bound) electron density inhibits runaway electrons in the current quench, as predicted. A physical model of radiative cooling has been developed and is validated against DIII–D experiments. The model shows that gas jet mitigation, including runaway suppression, extrapolates favorably to burning plasmas where disruption damage would be more severe. The use of real-time detection of the onset of a disruption to trigger massive gas injection and to mitigate the ensuing damage is demonstrated.

1. Introduction

Solving the problems associated with disruptions is a critical issue for advancing the tokamak concept as a viable magnetic fusion energy source. The magnitude of the damaging effects caused by disruptions increases with the plasma's thermal and magnetic energy. Disruptions are a particular concern for planned burning plasma experiments such as ITER [1] and FIRE [2]. While a high-energy density plasma is needed for fusion burn, it also becomes possible that a single-event uncontrolled disruption will terminate the operational viability of the wall components. Since these burning plasma experiments must be exploratory in nature in order to determine the optimal operational configuration for fusion gain, there will be an inherently greater risk of triggering instabilities that cause disruptions. A production reactor, however, will likely operate a safe distance from known limits.

Clearly the first priority in solving the disruption issue is to avoid the disruptions all together by means of active and accurate plasma control. However, in the case of off normal events it is then necessary to mitigate the damage that would be caused by the impending disruption. This is typically accomplished by purposefully triggering a plasma termination by a large injection of impurities [3–6], thus dissipating the plasma energy by relatively benign radiation. This technique is deemed successful if it maintains the operational viability of the fusion device. The mitigation is particularly focused on damage to internal components. The damages occurs principally by three means: 1) plasma-conducted/convected thermal loading of wall surfaces during the thermal quench, in particular the divertor targets, 2) **J×B** forces from vessel poloidal halo currents during the current quench and 3) the conversion of toroidal plasma current into relativistic runaway electrons (RE) that eventually are stopped by the wall, causing localized damage.

We will describe the use of high pressure jet injection of moderate-Z noble gases to provide disruption damage mitigation on the DIII–D tokamak [7].

2. Description of DIII-D Gas Jet Experiments

The gas jet consists of a 70 bar gas reservoir (at room temperature, 300 K) equipped with a fast-acting solenoid valve (opening time ~ 1 ms). The valve is recessed in an outboard radial

port adjacent to the DIII–D plasma [Fig. 1(a)]. The valve releases ~4×10^{22} particles (atoms or molecules) in ~2–5 ms into the port which effectively acts as a nozzle for the jet (diameter = 0.15 m, length ~ 0.5 m). We estimate the gas jet neutral density, n_0~4×10^{24} 20 m^{-3} and ram pressure $P=n_0T=\rho v^2$~30 kPa on entering the plasma. A pressure gauge at the valve opening confirms that pressures are the same for the different gases injected for these experiments: deuterium (D_2), helium (He), neon (Ne), and argon (Ar). The effective impurity atom density in the 35 m^3 DIII–D plasma volume is then ~1×10^{21} m^{-3}, or about 35 times the electron inventory of the target plasma.

The target DIII–D lower single-null diverted plasmas used in this study have the following parameters: major/minor radius, R/a = 1.7/0.6 m, plasma current, I_p ~ 1.5 MA, toroidal field B_T = 2.1 T, neutral beam heating power, P_{NBI} ~ 5–7 MW, electron density, n_e ~3×10^{19} m^{-3}, electron temperature $\langle T_e \rangle$ ~ 1.5 keV, $T_{e,central}$ ~ 3 keV, electron pressure $\langle P_e \rangle$ ~ 7 kPa. Target plasmas have total stored energy of W ~ 2.4 MJ with thermal (or kinetic) energy component, W_{th} ~ 0.6–0.8 MJ and poloidal magnetic energy, W_{mag} ~ 1.6 MJ.

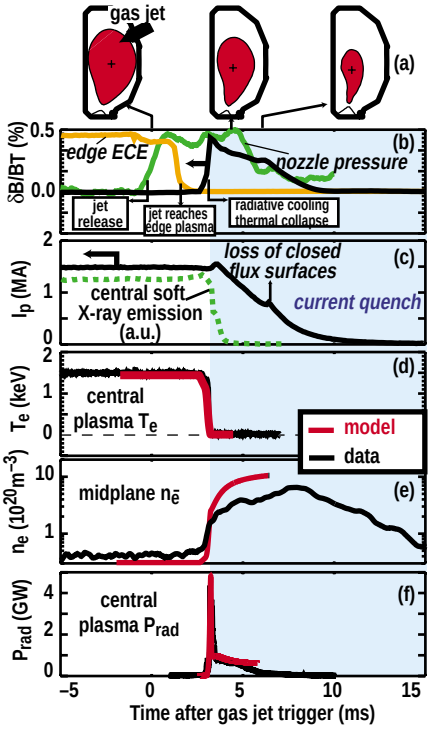

Fig. 1. Neon gas jet injection into a stable, neutral-beam heated plasma. (a) Jet geometry and evolution of plasma shape through current quench (shaded region). (b) Jet propagation through the nozzle is indicated by pressure near the valve and density cutoff of edge plasma electron cyclotron emission (ECE). Propagation through the plasma occurs without significant magnetic fluctuations ($\delta B/B_T$) until the radiative collapse. (c) Plasma current (I_p) and central plasma soft X-ray emission. (d) Central plasma electron temperature, T_e, (e) electron density, n_e and (f) radiated power, P_{rad}, are compared to KPRAD modeling results in red (see Section 4).

3. Mitigation of Disruption Damage

3.1. Gas Jet Injection into Stable Plasmas

High-pressure gas jet injection into a stable plasma rapidly dissipates the target plasma energy by radiation and provides a clean rapid quench of the plasma current. An example case of a pre-emptive neon gas jet injection into a stable plasma is shown in Fig. 1. Following the opening trigger to the valve, the jet begins to travel through the port/nozzle as indicated by the fast pressure increase near the valve. The density cutoff of edge 2nd harmonic ECE indicates the arrival of the jet front at the edge plasma ~ 1.5 ms later. After another 1.5 ms interval, the jet arrives at the central plasma (nozzle length ~ minor radius). Despite the presence of the jet in the plasma, no significant MHD activity ($\delta B/B_T$) occurs until the very large radiation (P_{rad}) arises from the centrally deposited neon, which collapses the plasma T_e and β in ~ 0.2 ms. A rapid exponential current decay is initiated by the thermal collapse and the plasma continues to radiate ~ 1 GW power. Electron density, n_e, increases by an order of magnitude to ~ 7×10^{20} m^{-3} in a few milliseconds. The core plasma remains well centered in the vessel throughout the current quench until closed flux surfaces are lost. Measured energy balance, which is accurate to within ~100 kJ, indicates that >95% of the initial energy of the target plasma is dissipated by radiation.

It is very important to note that no collateral damage is caused by the jet injection, either to pumping systems (the vessel pressure is raised to only ~10 Pa by the injection) or other internal systems. Subsequent discharges following the gas jet injection show no indication of radiation from the injected impurity species (following the standard intrashot 5 min helium glow discharge) with good control of density during the breakdown and current rampup. Typically, neon and argon are desorbed from wall surfaces in discharges following Ne/Ar

trace injection into stable, hot plasmas. Their absence in the gas jet case indicates that the radiatively collapsed plasma is too cold to provide sufficient plasma-wall sheath potential for ion implantation of the noble gases.

3.2. Gas Jet Penetration

The gas jet is found to penetrate through the plasma at approximately the sonic speed for all gases injected, delivering to the hot central plasma the large quantity of impurity needed for effective disruption mitigation. A cold front, caused by dilution or radiation from deposited gas species, is followed through the plasma using several electron temperature diagnostics (Fig. 2). Electron temperature is a reliable means of following jet penetration since parallel temperature equilibration time (~ 10^{-6} s) is fast compared to jet penetration time (~10^{-3} s). The jet propagation is consistent both with measured transit velocity of the jet through vacuum and with the expected sound speed (e.g. c_s ~ 250 m/s for Ar). The various gases also follow closely the expected decrease in sound speed with atomic mass (A), namely $v_{jet} \propto A^{-1/2}$.

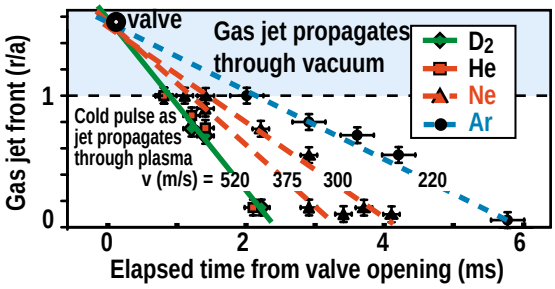

Fig. 2. Jet propagation for different injected gas species through vacuum (in nozzle) and central plasma. The cold front caused by the jet is measured by 2nd harmonic ECE density cutoff at edge of plasma (r/a=1), Thomson scattering T_e, soft X-ray emission and 3rd harmonic ECE in central plasma (no density cutoff for $n_e < 2.5\times10^{21}$ m^{-3}). Effective radial velocities are indicated.

3.3. Real-Time Disruption Detection and Mitigation

The DIII–D digital plasma control system (PCS) has been used to detect in real-time the onset of a vertical instability caused disruption, typically called a vertical displacement event, VDE (Fig. 3). The PCS triggers the injection of a neon gas jet when the plasma center moves past a variable threshold value set in the PCS for ΔZ_p, the vertical displacement of the plasma from its' equilibrium position. In these cases, vertical stability is intentionally disabled during the discharge to initiate the VDE. The time response of the PCS and gas jet is sufficient to terminate rapidly via radiation the plasma before the plasma moves down into the divertor floor. Similar detection algorithms have been developed and successfully tested for disruptions caused by density/radiative limits, although these results will not be described in detail here.

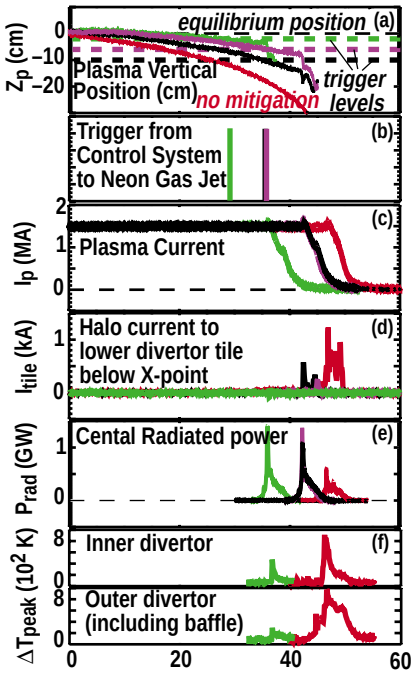

Fig. 3. Real-time detection and mitigation of downward-going vertical displacement event (VDE) disruptions. (a) Plasma center vertical position (Z_p) and ΔZ_p trigger levels set in plasma control system. Red lines: no mitigation, green lines: ΔZ_p = -2 cm, violet lines: ΔZ_p = –5 cm, black lines ΔZ_p = –10 cm. (b) Triggers to gas jet. (c) Plasma current. (d) Reduction of divertor halo currents below initial X-point position with mitigation (e) Increase of radiated power from core plasma with mitigation (f) Reduction of maximum divertor surface heating at inner and outer divertor with mitigation.

The neon gas jet substantially mitigates the damaging effects at the wall caused by the VDE. Thermal loading of the divertor is minimized by radiative dissipation of ~96% of the core plasma thermal energy. In contrast, a large portion of W_{th} is dissipated in the divertor volume by radiation or by heat

conduction to the floor in the non-mitigated case and little radiation occurs from the core plasma in the thermal quench. The reduction of heat conducted to the divertor reduces peak temperatures in the divertor by factors of 2 and 5 at the inner and outer divertor respectively. A summary of divertor conduction heat loading is shown in Fig. 4. The three typical natural (non-mitigated) disruption types find ~ 50%–100% of the plasma thermal energy directly lost to the divertor. The use of neon or argon gas jet clearly reduces this severe heat load problem, with the energy conducted to the divertor <10% W_{th}. Peak divertor tile temperatures are typical of those found for a large type-I ELM.

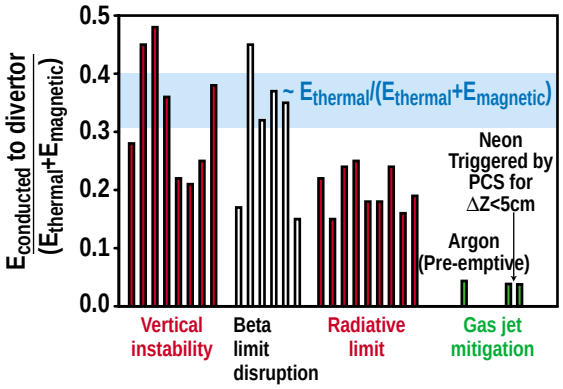

Fig. 4. Summary of divertor thermal load mitigation. The various classes of unmitigated disruptions shows total energy conducted to the divertor ~0.5–1 of the thermal energy of the target plasma. This is greatly reduced by the use of the neon or argon gas jet injection.

Vessel stresses caused by poloidal halo currents are reduced by a factor of four for these VDE cases (Fig. 3 and Fig. 5). Vessel stress is given by the product of peak poloidal halo current and toroidal peaking factor, both of which are reduced by a factor of two. Of particular importance, one finds halo currents essentially eliminated at regions outside the original location of the strikepoints (for example $I_{halo,tile}$ directly below the X–point in Fig. 3). This signifies that we expect reduced stresses on non-target locations in the divertor. Halo currents are reduced because the plasma current decays more rapidly than the plasma movement into the wall. This maintains high edge safety factor and minimizes conversion of toroidal current into poloidal halo current. For this reason the mitigation effectiveness is optimized when the gas jet is injected sooner into the vertically unstable plasma (i.e. the $\Delta Z_{threshold}$ is lower).

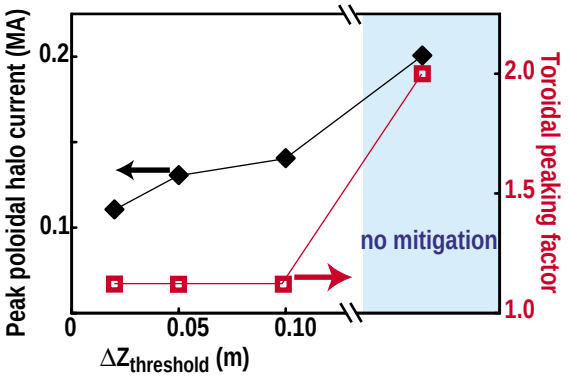

Fig. 5. Summary of halo current mitigation for VDE disruptions versus plasma vertical displacement trigger ΔZ_p for neon jet injection, and for the non mitigated case. The mitigation of peak poloidal halo current and the toroidal peak factor (measured at time of maximum stress to divertor) is optimal for lowest ΔZ (i.e. earliest stages of VDE).

3.4. Control of Runaway Electrons

A comparison of the argon pellet injection [8] and argon gas jet illustrates the effectiveness of the gas jet technique in controlling runaway electrons (RE) on DIII–D (Fig. 6). No significant population of RE has yet been observed for neon and argon gas jet injection on DIII–D, unlike the pellet which shows a confined RE current >100 kA in the current quench "tail" and the accompanying non-thermal soft X-ray emission. The two techniques both cause a rapid radiative cooling and current quench. The biggest difference between the techniques is that the gas jet injects ~100 times the number of atoms into the plasma volume. However, the gas jet creates only modestly higher free electron density increase in the plasma volume (ΔN_e), indicating that the average charge state of the neon is much lower in the gas jet case. One also sees that the current decay timescale ($\tau_{L/R}$) is very similar for the two cases, indicating that the accelerating parallel electric field, $E_{par} \propto 1/\tau_{L/R}$, is similar for the two cases. This is an important feature of the radiative mitigation techniques, particularly with regard to RE control, that will be addressed in the following section on modeling.

4. Modeling of Radiative Processes and Runaway Electrons

The KPRAD numerical simulation self-consistently evolves the impurity ionization state distribution and radiation/energy balance for impurity injection mitigation [9]. The code uses charge-state resolved atomic rate coefficients, including radiated power efficiencies L_{rad} (i.e. coronal equilibrium is not assumed). An example calculation for neon gas jet injection on DIII–D is shown in Fig. 7 and this simulation is compared to DIII–D experimental data in Fig. 1. This simulation uses volume-averaged target plasma parameters (no radial energy or particle transport). The jet species is deposited in plasma at sonic velocity.

One finds that the deposited gas impurity rapidly quenches the electron plasma kinetic energy through impurity line radiation. The strong electron-ion collisional coupling allows ion energy dissipation, and plasma temperature is decreased from several keV to $T_i = T_e \sim 3$ eV in ~ 0.2 ms, in agreement with data. The initial impurities to reach the plasma are burned-through to high charge states. However after the thermal quench further impurities deposited are only singly ionized and strong recombination in the high density plasma eliminates the higher ionization states. The radiation from the impurities is so overwhelming that the resulting cooling rules out significant further ionization. This effectively clamps the increase in free electron density at ~10^{21} m^{-3}, a key feature of the experimental data.

The total plasma current, I_p, cannot change on the short time-scale of the thermal quench. Therefore the thermal equilibrium of the current quench plasma ($W_{th} \sim 0$, $dW_{th}/dt \sim 0$) is determined by the equality of impurity-radiated power, P_{rad} [W m^{-3}] to ohmic heating, P_{ohmic} ($=\eta j^2$), namely

$$P_{rad} = \sum_i n_e n_{imp} L_{rad}(T_e, Z_i) \quad , \qquad (1)$$

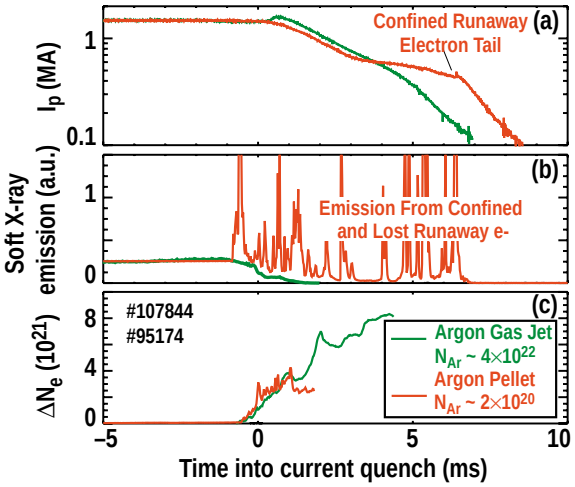

Fig. 6. Demonstration of runaway electron suppression for argon gas jet compared to argon cryogenic pellet injection. (a) Pellet case shows a confined runaway electron tail in plasma current. (b) In pellet case, soft X-ray emissions arise from confined runaways (continuous emission) and loss of runaway electrons to the wall (spikes in emission). (c) Increase in free electron density inventory in plasma (ΔN_e) indicates gas jet material is weakly ionized compared to pellet case.

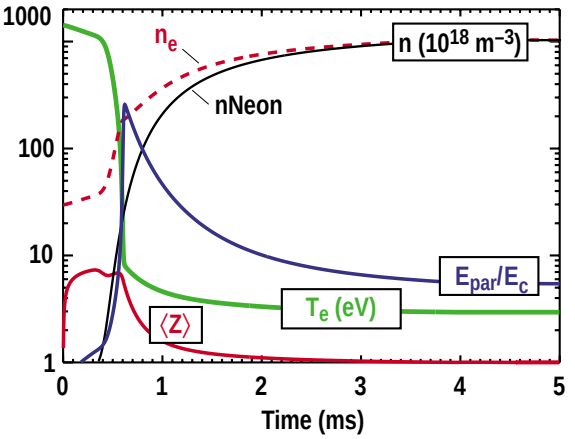

Fig. 7. Example of plasma/impurity thermal and ionization-state evolution from the KPRAD model for neon gas jet injection in DIII–D. The injected neon density (volume averaged from all charge states) n_{neon}, the free electron density n_e, electron and ion temperature (T_e, T_i), the average neon charge state, ⟨Z⟩, and the ratio of parallel electric field to critical electric field for runaway production (E_{par}/E_c) are shown (units as indicated). Model results of this run are compared to data in Fig. 1.

where n_e, n_{imp} [m^{-3}] are the free electron and impurity densities respectively, $L_{rad}(T_e, Z_i)$ [W m^3] is the collisional excitation radiative cooling rate of impurity Z in charge state i, and η [Ω m] is Spitzer resistivity. Eq. (1) determines T_e and parallel electric field, E_{par} through Ohm's law, namely $E_{par} = \eta\, j$. The reconnection event, evidenced by the sudden increase in δB (Fig. 1), flattens the current profile, yielding a constant inductance of L = 1.5 μH for DIII–D case.

We validate the model predictions of $\tau_{L/R} \propto 1/E_{par}$ and average impurity charge state $\langle Z \rangle$ against experimental data in Fig. 8. The model matches well the experimental trends and quantities over the wide range of n_{imp} found between the pellet and gas jet cases and the different injected species. The most important feature of the model and data is that E_{par} remains essentially constant over an extremely large range of n_{imp} and is sensitive only to the injected species. We can understand this from examining the radiative cooling rate curves for different species (Fig. 9). The equilibrium point between radiated power loss and Joule heating lies well below the ionization potential, I, of each of the species. In this case the functional dependence of the radiated power efficiency is $L_{rad} \propto \exp(-I/T_e)$. From Eq. (1) we can then see that T_e, which determines E_{par}, depends mostly strongly on I (i.e. species) and only logarithmically with other parameters such as n_{imp}, n_e, etc. We note that Spitzer resistivity has previously been verified experimentally in DIII–D during the current quench of a gas jet injection [10]. Therefore, the independent confirmations of η, E_{par} and Z in Fig. 8 also validate the calculated T_e.

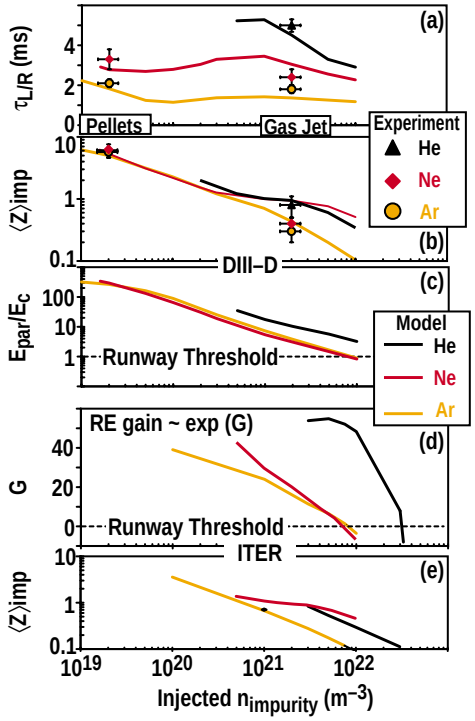

Fig. 8. (a–c) Comparison of KPRAD model to experimental results from DIII–D versus plasma volume averaged density of injected impurity, n_{imp}. (a) The L/R current decay time $\tau_{L/R} \propto 1/E_{par}$. (b) Average impurity charge state, $\langle Z \rangle_{imp}$, (c) Ratio of parallel electric field to critical electric field for runaway production (E_{par}/E_c). (d–e) KPRAD results for ITER with <T> = 10.5 keV, V=1890 m^{-3}, j = 0.55 MA m^{-2}, R,a= 8,2.8 m, L=13 μH. (d) Runaway gain amplification exponent (G) and (e) average charge state.

Relativistic runaway electrons (RE) are produced when E_{par}, which accelerates electrons, is greater than the critical electric field, E_c, set by collisional drag, namely E_c [V/m] = $mc\nu/e \sim 10^{-21} n_{e,T}$. The definition of $n_{e,T}$ includes *both* free, n_e, and bound electrons since both contribute to collisional drag of relativistic electrons [11]. RE experience amplification via the knock-on avalanche process in the current quench. Total RE amplification factor is given by e^G, where the amplification exponent $G = \gamma_{RE} \tau_{L/R} \propto \gamma_{RE}/E_{par}$ and the RE growth rate $\gamma_{RE} \propto (E_{par}/E_c - 1)$ [12]. Therefore runaway electrons and their amplification are suppressed when $E_{par}/E_c < 1$ (i.e. the Dreicer evaporation criterion is broken).

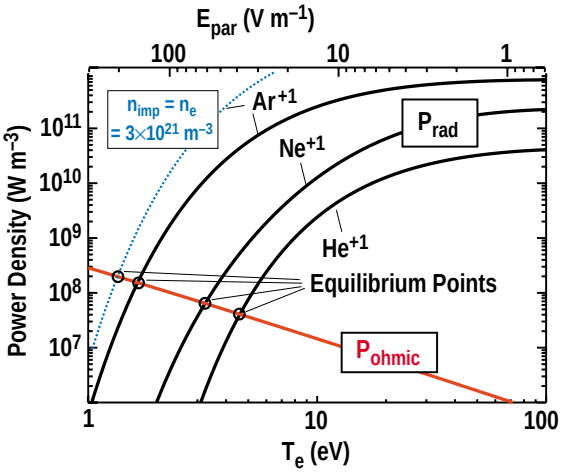

Fig. 9. Current quench T_e (or E_{par}) is determined by the crossing of ohmic and radiated power densities for singly ionized noble gases. Case shown: $n_{imp} = n_e = 10^{21}$ m^{-3}, j = 10^6 A m^{-2}, Z_{eff} = 1, except dotted line for Ar^{+1} with $n_{imp} = n_e = 3\times10^{21}$ m^{-3} indicating insensitivity of T_e to n_{imp}.

The RE amplification gain is calculated in the mitigation scenarios from the benchmarked KPRAD disruption model results (E, τ_{CQ}, etc.) and the analytic growth rate formula from [12] for both DIII–D and ITER [Fig. 8(d)]. The model indicates RE suppression ($E_{par}/E_c < 1$) to occur with $n_{imp} > 7\times10^{21}$ m^{-3} using gas jets of neon or argon in both devices. This is only a factor of three larger than our current experimental value, $n_{imp} \sim 2\times10^{21}$ m^{-3}. This result arises primarily from the increasing neutral gas density as n_{imp} is increased and $\langle Z \rangle$ decreases. Meanwhile, the

accelerating E_{par} is nearly constant as n_{imp} increases (as explained above). Therefore, $n_{e,T}$ and E_c can in a sense be "arbitrarily" increased by orders of magnitude by the large n_{imp} from the gas jet. At lower values of n_{imp} (e.g. pellet injection), we recover the previous result that RE amplification is so large (e^{40}) that the majority of plasma current will convert into relativistic electrons. We note that RE are suppressed in DIII–D experiments at a lower value of n_{imp} than predicted by the model. This is likely a consequence of the finite transport losses of RE [13], which are not considered in our calculations, and which makes the model a conservative estimate of the necessary n_{imp} for RE suppression. The DIII–D results suggest RE suppression occurs if the exponential gain factor $G < 5$. Neon plus argon are efficient at suppressing RE compared to He because of the larger number of bound electrons per atom. Additionally neon and argon provide good thermal mitigation due to their high radiation efficiencies.

5. Discussion

The essential goal of disruption mitigation is to dissipate the plasma energy by relatively benign isotropic radiation uniformly to the plasma-facing surfaces while avoiding halo currents and runaways. Gas jet injection mitigation as demonstrated on DIII–D clearly succeeds in this goal since the radiated power from the injected impurity competes against the heat conduction time scale as seen in natural disruptions or ELMs (~ 0.5 ms). Importantly, the jet itself does not seem to trigger large MHD activity until the impurity has been deposited in the plasma and allowed to dissipate the thermal energy by radiation.

The KPRAD model demonstrates that this rapid cooling and mitigation of thermal loading is also possible in the burning plasma environment, where <T> ~ 10 keV. Figure 10 shows an example KPRAD case of neon and helium gas jet mitigation in ITER (Q=10 target plasma). The only constraint on the model was that the injected impurity concentration was sufficient to dissipate the plasma thermal energy in < 1 ms. The wall temperature evolution was calculated from the KPRAD calculated time history of the radiated power spread uniformly over the first wall area through the thermal and current quench and the known thermal properties of the materials [14]. One finds a narrow, but accessible range of n_{imp} where the first wall material does not melt, and runaway electrons are controlled (see Fig. 8 for runaway suppression).

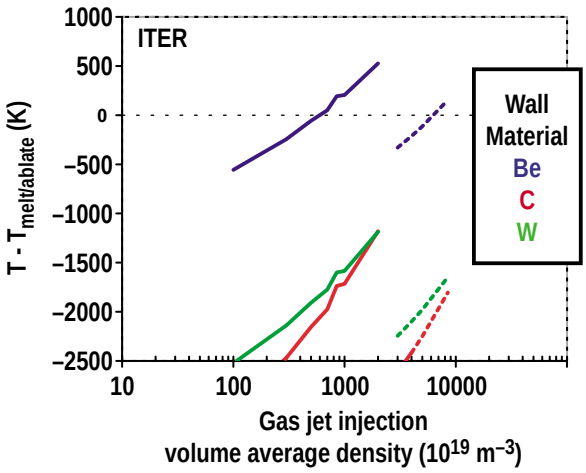

Fig. 10. KPRAD simulation results of maximum first wall surface temperatue for candidate wall material using neon (solid lines) or helium (dashed lines) gas jet mitigation. Peak surface temperature is shown relative to melting or ablation temperature of respective materials.

Efficient penetration of the gas jet to the central plasma seems to play an important role in the effectiveness of mitigation. While a fully developed model on gas jet penetration is not yet available, we hypothesize that the gas penetration is due to the high local neutral pressure and density of the jet. We note that the gas jet ram pressure exceeds the target plasma pressure and is on the order of the recoil pressure expected from the liquid jet model of Parks [15]. Further modeling and experiments on this subject are planned. If we assume that jet pressure versus plasma/recoil pressure is the key scaling parameter, we can speculate as to the needed pressure on a burning plasma experiment such as ITER. This scaling tells us that a factor of 10–100 fold pressure increase from the DIII–D gas jet is needed (P_{jet} > 1 Mpa). Restricting the injection cross-section with a specifically designed nozzle (rather than just the vacuum port) and moving the jet valve/reservoir close to the plasma will readily accomplish this.

6. Conclusions

High-pressure gas injection of moderate-Z noble gas has been used on the DIII–D tokamak to mitigate simultaneously the three major damage concerns in a tokamak caused by disruptions. First, divertor thermal loading is reduced by delivering large quantities of impurity into the core plasma to dissipate >95% of the plasma energy to the first wall. Secondly, vessel J×B stresses from poloidal halo currents are reduced. The rapid energy quench provided by the gas jet injection leads to a uniform resistive plasma that remains centered in the vessel while the toroidal current decays. Thirdly, the large volume density of bound electrons produced by the gas injection suppresses the generation of runaway relativistic electrons in the current quench.

A disruption detection algorithm has been successfully implemented in the DIII–D plasma control system. The onset of a vertical displacement event disruption was detected in order to trigger the gas jet injection. The plasma was rapidly and safely terminated by the jet, substantially reducing thermal and mechanical loading of the wall compared to an unmitigated disruption.

A physical model that describes the thermal and ionization balance of the plasma and gas jet material has been successfully validated against DIII–D experimental data. The model predicts that a gas jet will effectively mitigate disruption damage in burning plasma experiments such as ITER, including full suppression of runaway electrons. Further work is needed on the understanding and extrapolation of the gas jet penetration through the core plasma of a burning plasma device.

Acknowledgment

We acknowledge the assistance of G. Garstka and M. Austin. Work supported by U.S. Department of Energy under Grant DE-FG03-95ER54294, and Contracts DE-AC05-00OR22725, DE-AC03-99ER54463, and W-7405-ENG-48.

References

[1] ITER Physics Expert Groups, Nucl. Fusion **39**, (1999) 2577.
[2] D.M. Meade, Fusion Technology, **39** (2001) 36.
[3] P.L. Taylor, *et al.*, Phys. Plasmas **6**, (1999) 1872.
[4] R. Yoshino, T. Kondoh, Y. Neyatani, K. Itami, Y. Kawano, N. Isei, Plasma Physics and Controlled Fusion **39** (1997) 313.
[5] K.H. Finken, G. Mank, A. Kramer-Flecken, R. Jaspers, Nucl. Fusion **41** (2001) 1651.
[6] G. Pautasso, C. Tichmann, S. Egorov, T. Zehetbauer, O. Gruber, M. Maraschek, K.-F. Mast, V. Mertens, I. Perchermeier, G. Raupp, W. Treutterer, C.G. Windsor, Nucl. Fusion **42** (2002) 100.
[7] J. L. Luxon, Nuclear Fusion **42** (2002) 614.
[8] T.E. Evans, *et al.* Proc. 17th IAEA Fusion Energy Conf., Yokohama, Japan, 1998 (International Atomic Energy Acency, 1999), CSP-1P/EXP3/07 p. 847.
[9] D.G. Whyte, *et al.*, Proc. of 24th European Conference on Controlled Fusion and Plasma Physics, Berchtesgaden, Germany, 1997, Vol. 21A (European Physical Society, 1997) p. 1137.
[10] D.A. Humphreys, D.G. Whyte, Phys. Plasmas **7**, (2000) 4057.
[11] P.B. Parks, M.N. Rosenbluth, S.V. Putvinski, Phys. Plasmas **6**, (1999) 2523.
[12] M.N. Rosenbluth and S.V. Putvinski, Nucl. Fusion **37**, (1997) 1355.
[13] R. Yoshino, S. Tokuda, Y. Kawano, Nucl. Fusion **39** (1999) 151–161.
[14] B.V. Kuteev, V. Yu Sergeev, S. Sudo, Nucl. Fusion **35**, (1995) 1167.
[15] P.B. Parks, M.N. Rosenbluth, S.V. Putvinski, T.E. Evans, Fusion Technology, **35** (1999) 267.